Journal of Materials Science and Chemical Engineering, 2023, 11, 1-13
https://www.scirp.org/journal/msce
ISSN Online: 2327-6053
ISSN Print: 2327-6045

Structural Analysis of TiC and TiC-C Core-Shell Nanostructures Produced by Pulsed-Laser Ablation

Luis Enrique Iniesta Piña[1], Miguel Ángel Camacho López[2*], Rafael Vilchis Néstor[3], Víctor Hugo Castrejón Sánchez[4], Delfino Reyes Contreras[5*]

[1]Mestría en Ciencia de Materiales, Facultad de Química, Campus Rosedal, Universidad Autónoma del Estado de México, Toluca, México
[2]Laboratorio de Fotomedicina, Biofotónica y Espectroscopía Láser de Pulsos Ultracortos, Facultad de Medicina, Universidad Autónoma del Estado de México, Toluca, México
[3]Centro Conjunto de Investigación en Química Sustentable, UAEM-UNAM, Toluca, México
[4]TecNM/Tecnológico de Estudios Superiores de Jocotitlán, Jocotitlán, México
[5]Laboratorio de Acústica y Nanomateriales, Facultad de Ciencias, Campus el Cerrillo, Universidad Autónoma del Estado de México, Toluca, México
Email: *mikentoh@hotmail.com, *dreyesc@uaemex.mx

How to cite this paper: Iniesta Piña, L.E., Camacho López, M.Á., Vilchis Néstor, R., Castrejón Sánchez, V.H. and Reyes Contreras, D. (2023) Structural Analysis of TiC and TiC-C Core-Shell Nanostructures Produced by Pulsed-Laser Ablation. *Journal of Materials Science and Chemical Engineering*, **11**, 1-13.
https://doi.org/10.4236/msce.2023.117001

Received: May 29, 2023
Accepted: July 11, 2023
Published: July 14, 2023

Abstract

This paper reports on the ablation process of a pure Ti solid target immersed in a C-enriched acetone solution, leading to the production of titanium carbide (TiC) and Ti-C core-shell nanostructures. The used route of synthesis is generally called pulsed laser ablation in liquid (PLAL). The presence of carbon structures in the solution contributed to the carbon content in the produced Ti-based nanomaterials. The atomic composition of the produced nanostructures was analyzed using SEM-EDS, while TEM micrographs revealed the formation of spherical TiC and core-shell nanostructures ranging from 40 to 100 nm. The identification of atomic planes by HRTEM confirmed a 10 nm diameter C-shell with a graphite structure surrounding the Ti-core. Raman spectroscopy allowed for the identification of D and G peaks for graphite and a Raman signal at 380 and 600 cm^{-1}, assigned to TiC. The results contribute to the state-of-the-art production of TiC and Ti-C core-shell nanostructures using the PLAL route.

Keywords

Laser Ablation, TiC, Nanoparticles, Core-Shell Nanoparticles, Pulsed Laser

1. Introduction

Pulsed laser-materials processing is a continuously growing and updating me-

thod for the production of nanoscale materials, including metals [1] [2], oxides [3] [4], carbon [5] [6], and others. It is based on the interaction of laser pulses with solid targets [3] [6], suspended materials [7] [8], or even pure liquids [9]. This route is generally referred to as pulsed laser ablation in liquid (PLAL). In this process, the laser pulse energy is transferred to the material of interest, ablating or fragmenting the target or suspended matter and/or ionizing the liquid, generating products for the growth of nanomaterials.

Titanium carbide (TiC) is a ceramic material that exhibits interesting physical and chemical properties, such as high hardness, electrical and thermal conductivity, and resistance to oxidation and corrosion at high temperatures [10]. Several studies have shown that obtaining a complete stoichiometric ratio of TiC is challenging; the stable stoichiometric ratio x of TiC_x can range from $0.48 < x < 0.98$. TiC crystallizes in the NaCl-type structure with a face-centered cubic (FCC) lattice, where sites are alternately occupied by metallic and non-metallic atoms, respectively [11]. It is known that TiC-growth, as nanomaterial morphologies can be cubes, truncated octahedrons, sphericities, dendrites, and different dimensional morphologies, such as nanorods, nanosheets, and nanospheres, can be obtained under different reaction conditions [12] [13].

The synthesis route for Ti-C nanoparticles has specific requirements for the growth of this type of ceramic, as the reaction between Ti and C cannot occur unless at high temperatures (greater than 3000 K). These high ignition temperatures, which are close to the melting point of titanium carbide, are challenging to achieve and can result in wasted energy [14] [15]. Therefore, many efforts have been made to produce this type of refractory metal ceramics, such as the carbothermal reduction process at lower temperatures using polymeric compounds and metal oxides as carbon sources [16], the wire burst or wire pulse discharge, industrial plasma method [17] [18], among others.

While the PLAL route has mainly been used to produce TiO nanostructures, some limited works have reported the production of TiC nanoparticles. It was reported the laser ablation of a TiC target in a liquid medium with laser pulses of 100 fs, wavelength of 800 nm, and pulse energy of 3 mJ in water, acetone, n-hexane, and toluene [19]. This method allowed for the synthesis of nanoparticles of titanium carbide (TiC) in carbon-rich liquid media, as well as titanium dioxide (TiO_2) for oxygen-rich liquid media. The solid target can only be Titanium, and still get TiC nanoparticles, indicating that the liquid medium influences the synthesis process [20]. Recently, the presence of TiC structure was reported on the surface of laser-ablated samples in toluene, n-hexane, and n-heptane [21], as well as the production of TiO_2@TiC core-shell structures in spheres with sizes of 200 - 350 nm, decorated with −2 nm ultrasmall Pt NPs [22].

This paper reports on the production of TiC and related nanostructures through the PLAL method using ps laser pulses to ablate a Ti solid target while immersed in a carbon-rich acetone liquid ambient. The ablation products were structurally characterized using SEM-EDS, TEM-HRTEM, and Raman micro-

scopy. The structural analysis confirmed the formation of Ti-based nanomaterials, such as TiC, and core-shell Ti-C, nanoparticles. These results contribute to the state-of-the-art production of TiC and Ti-C or TiC-C core-shell nanostructures using the PLAL route.

2. Experimental Details

2.1. Laser Ablation of Solids in Liquid Media Process

The pulsed laser ablation of solid in liquids media (PLAL) process for synthesizing titanium carbide (TiC) nanoparticles was performed using a typical experimental setup for this method [2] [6], as described in **Figure 1**. A Nd:YAG pulsed laser (EXPLA) operating at its fundamental emission line (1064 nm), with a pulse width of 150 ps, a per-pulse laser energy of 30 mJ, and a 10 Hz repetition rate, was focused down with a 30 cm lens on the surface of a solid carbon target (Kurt Lesker, 99.999% pure) while immersed in 20 ml of pure acetone (Sigma Aldrich) for 10 minutes. The ablation process allowed the obtaining of a carbon nanostructure-based colloidal solution. In the second step, a pure Ti solid target (Kurt Lesker, 99.9999% pure) was immersed in the described carbon colloid, inducing the ablation process for 10 minutes under the same irradiation parameters. The obtained colloid then contained C and Ti nanostructures, and due to the reactive process, TiC and core/shell Ti/C structures were formed, as shown below. For comparison, the ablation process of the pure Ti target immersed in acetone was also performed.

2.2. Structural Characterization

Structural characterization of the as-prepared nanoparticles was performed using scanning electron microscopy coupled with energy dispersive spectroscopy (SEM-EDS), transmission electron microscopy (TEM), and high-resolution

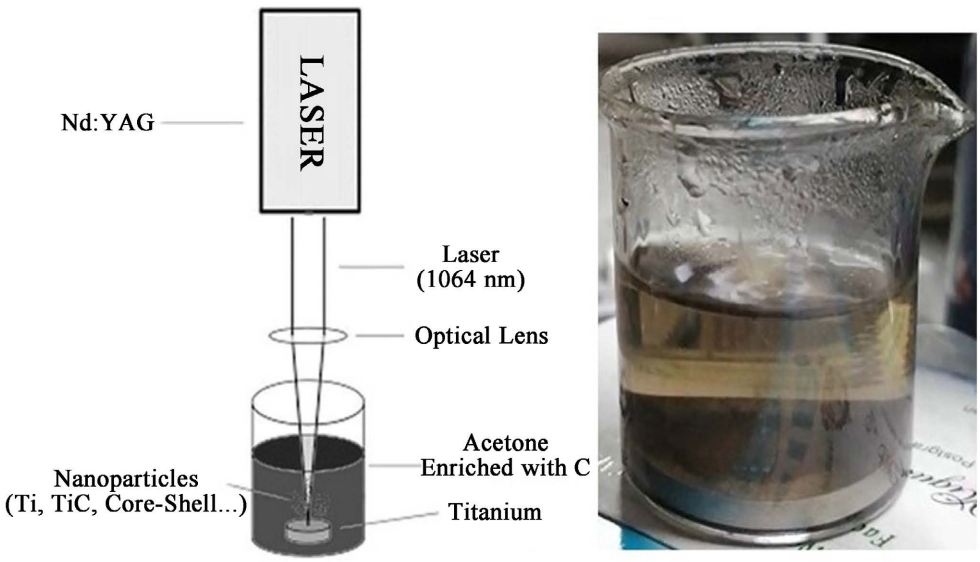

Figure 1. Experimental setup for the PLAL method to obtain the Ti-based nanomaterials.

transmission electron microscopy (HRTEM). Raman spectroscopy was also used to provide a complete analysis. The structural analysis was conducted only for the Ti-ablated sample in the C-enriched acetone ambient.

SEM-EDS analysis was performed using a JOEL-JSM IT-100 microscope operating in high vacuum with an acceleration voltage of 20 kV. EDS allowed for the determination of the elemental composition of the products obtained, as well as their percentages. For TEM characterization, 0.05 g of each sample was placed on Cu-grids coated with carbon, and three drops of the solution were evaporated on the grid to leave behind the TiC nanoparticles. TEM and HRTEM measurements were carried out using a JEOL-2010 electron microscope at an accelerating voltage of 200 kV.

Raman analysis was conducted using a Raman Horiba Jobin Yvon equipment model XPLORA-PLUS equipped with a laser with a wavelength of 780 nm as an excitation source, with a nominal power of 0.2 mW. The laser beam was focused on the samples with a 50× objective, which also served to collect the scattered light and direct it to a charge-coupled device (CCD) camera. Analysis was performed over a range of 300 - 2300 cm^{-1} to identify the corresponding Raman peaks.

3. Results and Discussion

3.1. SEM-EDS

Figure 1 shows the dark-brown solution obtained after the pulsed laser ablation process, which contains both C- and TiC-nanoparticles, due to the synthesis process described in section 2.1. A SEM micrograph is displayed in Figure 2. The material collected for SEM analysis was obtained from the bottom of the container after full acetone evaporation, and it was collected by scraping material

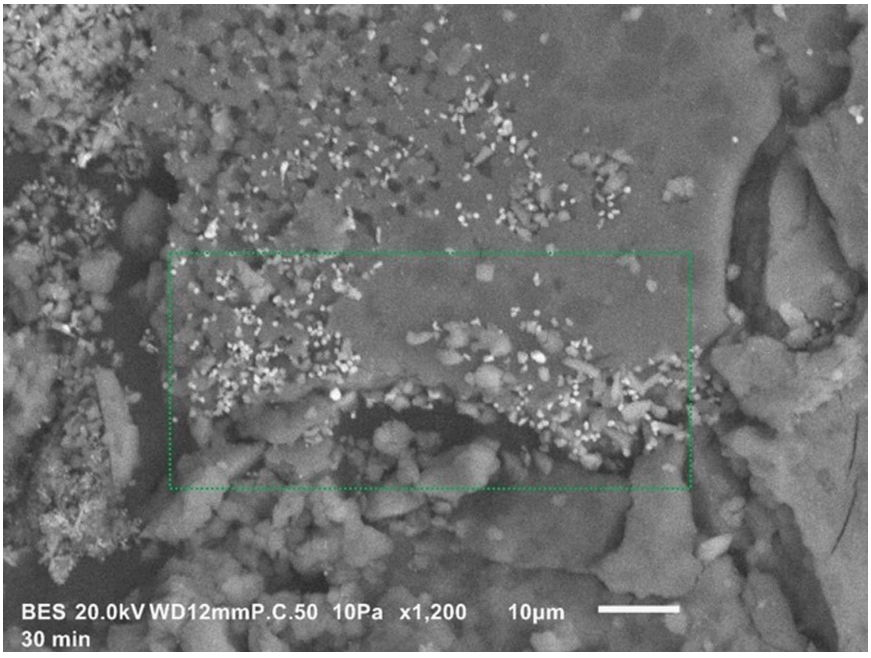

Figure 2. SEM micrograph for the C-enriched Ti-ablated sample.

with a spatula. Figure 2 shows a topographic picture of the ablated Ti in the presence of colloidal carbon sample with a ×1200 amplification. The micrograph shows an apparently solid structure with a size over 50 μm covered by irregular grey structures and white granular sphere agglomerates whose size can be estimated to be around 0.5 μm diameter. In addition to the topographic information from SEM, coupled EDS analysis is described above.

For EDS analysis, the selected area identified with the green rectangle in Figure 2 was used. From the analysis, it was found that the largest amount of material obtained is carbon, as shown in Figure 3(a) and Table 1. In atomic percentages, 58.83% is occupied by carbon, while titanium accounts for 10.28%. Oxygen was found to be 27.74%, and its presence can be attributed to a great extent to the fact that the ablation and analysis processes were not isolated. Likewise, in the dissociation process due to the laser-interaction, hydroxyl groups are found in acetone, from which oxygen can be released. Additionally, a smaller quantity of polluting elements such as silicon and sodium were recorded, which were attributed to the vial that contained the material, as the vial was scraped with a spatula during the process to obtain it. It is necessary to note a particular contaminant, chlorine, with a percentage of 1.82%, which makes it significant and abundant. This particular contaminant can be attributed to the drying process, where cleaning with chlorine was constant, so its vapor could have reached the samples and contaminated them significantly.

As mentioned earlier, SEM-EDS can obtain images with elemental maps so that the distribution of each element can be presented with different colors. The analysis was conducted on titanium and carbon. In the case of carbon, the area where it is found was assigned with green color, while titanium is red, as observed in Figure 3(b) and Figure 3(c). It can be observed that the agglomerates with a lighter tone are registered in the image, and this abundance of the metal can be corroborated with the composition spectrum of Figure 3(a). These results indicate the presence of both carbon and titanium as products of the fragmented material and in the agglomerates, as expected. From the images, we can get an idea of the structures formed. Within the Ti-ablated material and due to the amount of carbon and titanium, it is expected to find both TiC and Ti-C core-shell nanoparticles.

3.2. Transmission Electron Microscopy

In Figure 4, micrographs obtained from TEM characterization reveal the presence of both large and small nanoparticles. The larger nanostructures appear to be nearly perfect spheres of varying sizes. Figure 4(a) and Figure 4(b) depict two distinct nanoparticles with diameters of 50 nm and 100 nm, respectively. This size is also observed in Figure 4(c) and Figure 4(d), where particles less than 40 nm can be observed in Figure 4(c) and a not well-shaped structure, along with another particle whose size is less than 40 nm, can be seen in Figure 4(d). These nanostructures appear to be surrounded by smaller nanoparticles,

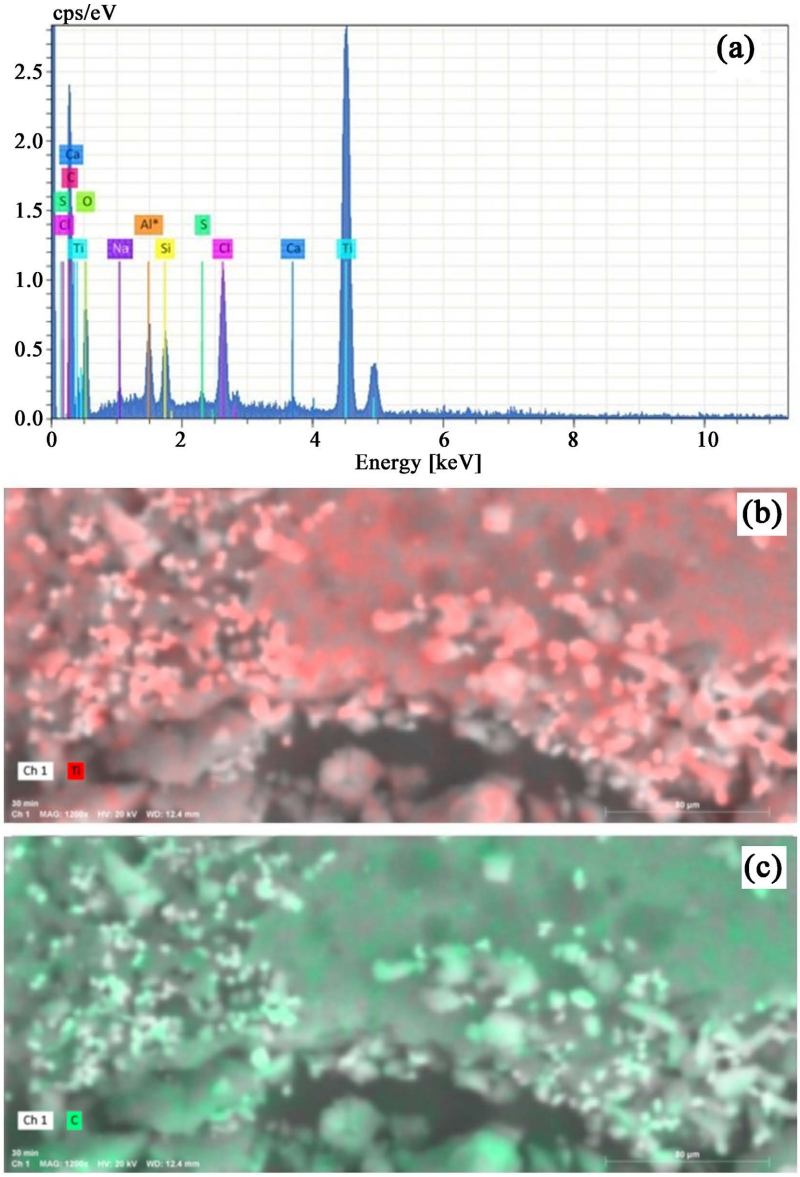

Figure 3. (a) EDS-analysis for the abundance of the elements composing the sample from **Figure 2**; (b) EDS color maps for Ti tanium and (c) for carbon.

Table 1. Percentage of each element present in the sample obtained from EDS analysis.

Element	Atomic %	Absolute error %	Relative error %
Titanium	10.28	0.98	2.90
Chlorine	1.82	0.18	4.15
Silicon	0.76	0.09	6.52
Sulfur	0.13	0.04	14.30
Sodium	0.31	0.07	13.98
Carbon	58.83	6.77	13.99
Oxigen	27.74	4.91	16.16
Calcium	0.12	0.04	12.81

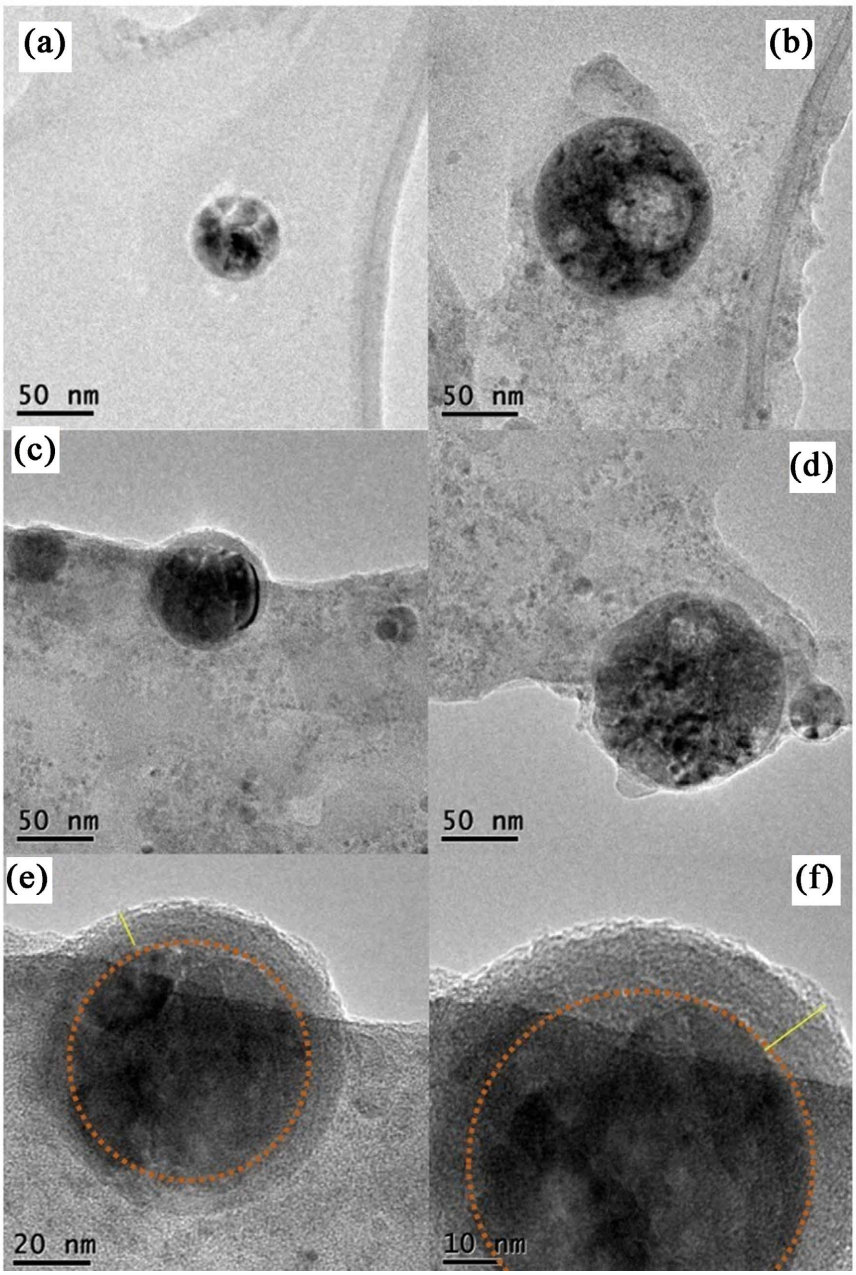

Figure 4. (a)-(c) Micrographs of a single TiC nanoparticles besaide C-nanoparticles; (d) Non-well shapped TiC nanoparticle; (e) and (f) Zoom of the nanoparticles in (c), where the core-shell structure is observed, which is easier to see due to the orange circle.

measuring just a few nanometers in size. According to reports on the production of C nanoparticles using the PLAL route, the synthesis process leads to the production of nanoparticles measuring less than 10 nm [6]. Therefore, these structures can be identified as entirely carbon nanostructures resulting from the previous C-enrichment process.

Zooming in on the nanoparticle in **Figure 4(c)** reveals that the nanostructures are embedded within a matrix, as depicted in **Figure 5(e)** and **Figure 5(f)**, with 20 nm and 10 nm scales, respectively. The appearance of the particle is similar to

that of core-shell nanostructures. As shown in these figures, the nanoparticles have a spherical section with a surrounding layer or shell (identified by the non-continuous orange line), which has a thickness of approximately 12 nm (indicated by the yellow line). Based on their observable features, the core is presumed to be composed of amorphous carbon, as will be demonstrated below through Raman analysis.

High-resolution TEM (HRTEM) images, as shown in **Figure 5**, allow for the observation of crystallographic planes of the produced nanoscale structures. The GATAN Digital Micrograph software was used to examine these planes and determine the distance between them. Micrographs with a 5 nm scale, shown in **Figures 5(a)-(c)**, reveal the crystallographic planes of Ti in its Hexagonal Close-Packed (HCP) structure [23]. The most important plane, (1 1 1), corresponding to the titanium carbide structure in its face-centered cubic (FCC) crystalline phase [24], was identified in **Figure 5(b)**. Additionally, the (0 0 2) plane, corresponding to graphite planes, was identified in **Figure 5(d)** [25]. However, no atomic planes were observed in the shell structure proposed as the carbon

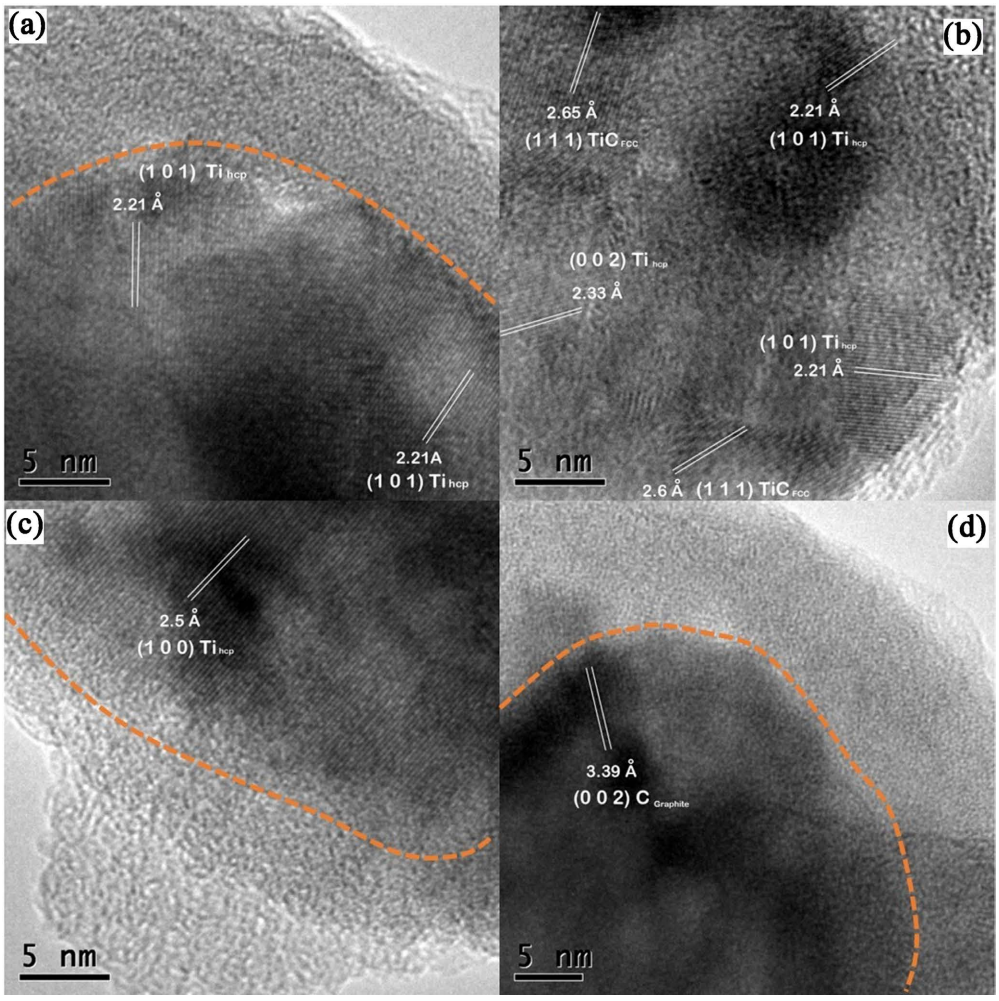

Figure 5. HRTEM micrographies, (a)-(c) contain the planes corresponding to Ti and TiC, and (d) is for the plane charactering the graphite.

shell, beyond the area where Ti and TiC planes were found (see orange line). This observation confirms the possibility of proposing the production of Ti-C core-shell or even TiC-C nanostructures. However, to strictly confirm this proposal, further characterization using XPS or XRD techniques is necessary, which is beyond the scope of the present work. **Figure 5** shows the atomic plane analysis, which strictly corresponds to TiC in the core part, while the amorphous structure is for amorphous carbon. The non-continuous dark pattern in the structure suggests that the C-shell structure may not be completely homogeneous, which has been previously reported in Cu-C core-shell nanostructures [26]. Besides that, a previous study reported the production of MoC-Graphite core-shell nanostructures in a carbon-enriched ambient [27], which is similar to what is being reported here and supports our proposed core-shellproduced nanostructure. This effect was also observed as descriptive evidence for the formation of Fe_3O_4/Ag core-shell nanoparticles [28].

3.3. Raman Analysis

Figure 6 displays the Raman spectrum of the produced nanostructures. The Raman shift related to the carbon signal has been fitted with four Lorentzian peaks, enabling identification of the main Raman peaks of the produced nanostructures. The G band, located at approximately 1590 cm^{-1}, corresponds to the E_{2g} vibrational mode and represents the stretching vibration of the sp^2-type hybridized carbon bonds in the graphite structure. Therefore, this band is indicative of the degree of crystallinity, unlike the D band [25]. The D band, located around 1378 cm^{-1}, is directly associated with the degree of structural disorder in graphite due to the loss of symmetry. This can be attributed to the stretching

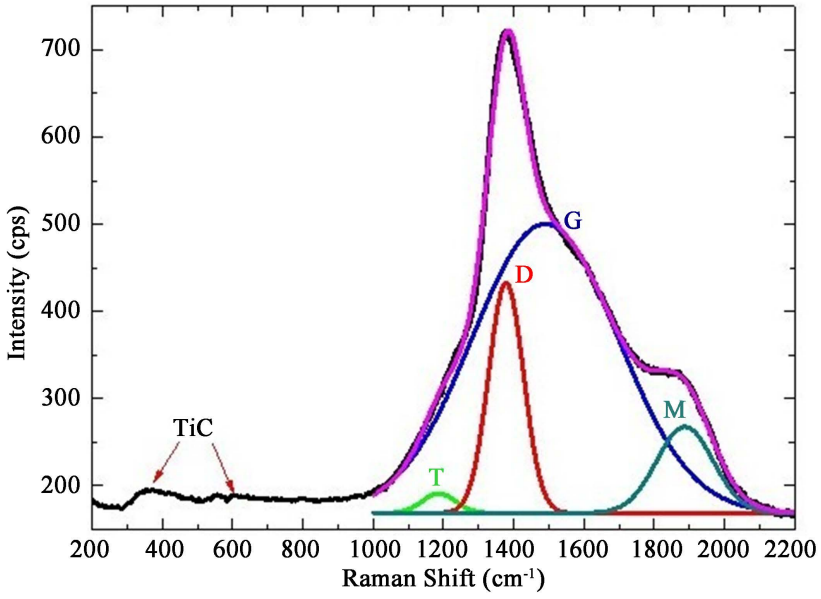

Figure 6. Raman analysis where D and G peaks for carbon structure and the corresponding to TiC were identified. Additional T and M peaks were observed and confirmed with the Lorentzian fitting.

vibration in the sp^2 and sp^3-type hybridized bonds of the carbon atoms. In simpler terms, it is due to amorphous carbon. As observed in the registered intensity, amorphous carbon is the most abundant compound in the substance [19] [27]. Two additional Raman peaks were recorded that are not usually reported for TiC-based nanomaterials and could be due to the C-enrichment process. The first band, assigned as T band, was identified at approximately 1170 cm^{-1} and is related to the presence of C-C bindings. The second band, at 1865 cm^{-1}, is a Raman peak overtone called M or D' + TA and is also related to the presence of C=C carbon bindings [29]. The high intensity of the D-band is associated with the presence of defects, disorder, or structural imperfections in the carbon lattice, which agrees with the amorphous shell observed in **Figure 5** TEM micrographs.

The small, not very intense bands recorded around 300 and 600 cm^{-1} in **Figure 6**, corresponding to the vibrational modes of non-stoichiometric TiC, is of particular interest, as it strictly confirms the presence of the produced TiC nanostructures. Stoichiometric TiC does not present Raman signals [30] [31]. The Raman signals recorded at 390 and 605 cm^{-1} identify the TiC nanostructures. However, they have low Raman intensity, which confirms that the bulk of the material target is stoichiometric TiC.

In addition, the ID/IG ratio, which is the ratio between Raman peak intensities, was calculated from the Raman results and found to be 1.52. This ratio was obtained from the raw data of the Raman equipment (719.581/473.152), and considered the photons reaching the detector. It is widely recognized that an increase in the ID/IG ratio corresponds to an increase in structural disorder or defect density in carbon materials. Higher values of ID/IG indicate the presence of defects, such as edge defects and vacancies, which occur in the case of amorphous graphite that lacks a regular crystalline structure [32].

4. Conclusion

The results demonstrate the possibility of obtaining TiC and core-shell-based Ti nanostructures using the PLAL route. This was achieved by ablating a pure Ti solid target immersed in a C-enriched acetone liquid media using ps laser pulses. From HRTEM, atomic planes for Ti, TiC, and graphite were identified, suggesting the production of TiC, Ti-C, and even TiC-C shell nanostructures using the PLAL technique. Even when a detailed analysis of these structures is outside the scope of this paper, our results confirm the formation of the TiC core covered by a disordered graphite structure. The results contribute to the state-of-the-art production of TiC and Ti-C core-shell nanostructures using the PLAL route and their potential applications.

Acknowledgements

L.E.I.P. thanks to CONACYT for the support in developing master studies. This research was partially supported by CONACYT grants 280518 and A1-S-34533.

Conflicts of Interest

The authors declare no conflicts of interest regarding the publication of this paper.

References

[1] Gaurav, K., Shukla, S., Sastikumar, D. and Koinkar, P. (2021) Progress in Pulsed Laser Ablation in Liquid (PLAL) Technique for the Synthesis of Carbon Nanomaterials: A Review. *Applied Physics A*, **127**, Article No. 810. https://doi.org/10.1007/s00339-021-04951-6

[2] Mateos, H., Picca, R.A., Mallardi, A., Dell'Aglio, M., De Giacomo, A., Cioffi, N. and Palazzo, G. (2020) Effect of the Surface Chemical Composition and of Added Metal Cation Concentration on the Stability of Metal Nanoparticles Synthesized by Pulsed Laser Ablation in Water. *Applied Sciences*, **10**, Article 4169. https://doi.org/10.3390/app10124169

[3] Menazea, A.A. (2020) One-Pot Pulsed Laser Ablation Route Assisted Copper Oxide Nanoparticles Doped in PEO/PVP Blend for the Electrical Conductivity Enhancement. *Journal of Material Research and Technology*, **9**, 2412-2422. https://doi.org/10.1016/j.jmrt.2019.12.073

[4] El-Faham, M.M., Mostafa, A.M. and Toghan, A. (2021) Facile Synthesis of Cu_2O Nanoparticles Using Pulsed Laser Ablation Method for Optoelectronic Applications. *Colloids and Surfaces A*: *Physicochemical and Engineering Aspects*, **630**, Article ID: 127562. https://doi.org/10.1016/j.colsurfa.2021.127562

[5] Mostafa, A.M., Mwafy, E.M., Awwad, N.S. and Ibrahium, H.A. (2021) Synthesis of Multi-Walled Carbon Nanotubes Decorated with Silver Metallic Nanoparticles as a Catalytic Degradable Material via Pulsed Laser Ablation in Liquid Media. *Colloids and Surfaces A*: *Physicochemical and Engineering Aspects*, **626**, Article ID: 126992. https://doi.org/10.1016/j.colsurfa.2021.126992

[6] Reyes, D., Camacho, M.A., Camacho, M., Mayorga, M., Weathers, D., Salamo, G., Wang, Z. and Neogi, A. (2016) Laser Ablated Carbon Nanodots for Light Emission. *Nanoscale Research Letters*, **11**, Article No. 424. https://doi.org/10.1186/s11671-016-1638-8

[7] Kanakkillam, S.S., Shaji, S., Krishnan, B., Vazquez, S., Aguilar, J.A., Mendivil, M.I. and Avellaneda, D.A. (2021) Nanoflakes of Zinc Oxide: Cobalt Oxide Composites by Pulsed Laser Fragmentation for Visible Light Photocatalysis. *Applied Surface Science*, **501**, Article ID: 144223. https://doi.org/10.1016/j.apsusc.2019.144223

[8] Reyes, D., Camacho, M., Buendía, L., Camacho, M.A., Squires, B. and Neogi A. (2022) Pulsed Laser Fragmented Carbon Black Powders for the Synthesis of Carbon Nanodots. *International Journal of Optics and Photonic Engineering*, **7**, Article ID: 047.

[9] Altuwirqi, R.M., Albakri, A.S., Al-Jawhari, H. and Ganash, E.A. (2020) Green Synthesis of Copper Oxide Nanoparticles by Pulsed Laser Ablation in Spinach Leaves Extract. *Optik*, **219**, Article ID: 165280. https://doi.org/10.1016/j.ijleo.2020.165280

[10] Rahim, G.A. and Arbey, J. (2013) Propiedades estructurales del carburo de titanio TiC. *Revista Colombiana de Física*, **45**, 181-183.

[11] Zhou, Y. and Sun, Z. (2000) Crystallographic Relations between Ti_3SiC_2 and TiC. *Materials Research Innovation*, **3**, 286-291. https://doi.org/10.1007/PL00010876

[12] Song, M.S., Huang, B., Huo, Y.Q., Zhang, S.G., Zhang, M.X., Hu, Q.D. and Li, J.G. (2009) Growth of TiC Octahedron Obtained by Self-Propagating Reaction. *Journal*

of Crystal Growth, **311**, 378-382. https://doi.org/10.1016/j.jcrysgro.2008.10.065

[13] Nie, J.F., Wu, Y.Y., Li, P.T., Li, H. and Liu, X.F. (2012) Morphological Evolution of TiC from Octahedron to Cube Induced by Elemental Nickel. *Crystal Engineering Communications*, **14**, 2213-2221. https://doi.org/10.1039/c1ce06205k

[14] Dong, B., Li, Q., Qiu, F. and Shu, S. (2019) The Synthesis, Structure, Morphology Characterizations and Evolution Mechanisms of Nanosized Titanium Carbides and Their Further Applications. *Nanomaterials*, **9**, Article 1152. https://doi.org/10.3390/nano9081152

[15] Ghosh, S., Ranjan, P., Kumaar, A., Sarathi, R. and Ramaprabhu, S. (2019) Synthesis of Titanium Carbide Nanoparticles by Wire Explosion Process and Its Application in Carbon Dioxide Adsorption. *Journal of Alloys Compounds*, **794**, 645-653. https://doi.org/10.1016/j.jallcom.2019.04.299

[16] Keller, T.M., Laskoski, M., Saab, A.P., Qadri, S.B. and Kolel, M. (2014) *In Situ* Formation of Nanoparticle Titanium Carbide/Nitride Shaped Ceramics from Meltable Precursor Composition. *Journal of Physics Chemistry*, **118**, 30153-30161. https://doi.org/10.1021/jp5082388

[17] Zuñiga, V.A., Shaji, S., Krishnan, B., Johny, J., Sharma, S., Avellaneda, D.A., Aguilar, J.A., Das, T.K. and Ramos, N.A. (2019) Synthesis and Characterization of Black TiO_2 Nanoparticles by Pulsed Laser Irradiation in Liquid. *Applied Surface Science*, **483**, 156-164. https://doi.org/10.1016/j.apsusc.2019.03.302

[18] Liu, P., Cai, W., Fang, M., Li, Z., Zeng, H., Hu, J., Luo, X. and Jing, W. (2009) Room Temperature Synthesized Rutile TiO_2 Nanoparticles Induced by Laser Ablation in Liquid and Their Photocatalytic Activity, *Nanotechnology*, **20**, Article ID: 285707. https://doi.org/10.1088/0957-4484/20/28/285707

[19] De Bonis, A., Santagata, A., Galasso, A., Laurita, A. and Teghil, R. (2016) Formation of Titanium Carbide (TiC) and TiC@C Core-Shell Nanostructures by Ultra-Short Laser Ablation of Titanium Carbide and Metallic Titanium in Liquid. *Journal of Colloid and Interface Science*, **489**, 76-84. https://doi.org/10.1016/j.jcis.2016.08.078

[20] Blažeka, D., Car, J. and Krstulović, N. (2022) Concentration Quantification of TiO_2 Nanoparticles Synthesized by Laser Ablation of a Ti Target in Water. *Materials*, **15**, Article 3146. https://doi.org/10.3390/ma15093146

[21] Feizi, B., Jaleh, B., Kakuee, O. and Fattah, A. (2019) Formation of Titanium Carbide on the Titanium Surface Using Laser Ablation in n-Heptane and Investigating Its Corrosion Resistance. *Applied Surface Science*, **478** 623-635. https://doi.org/10.1016/j.apsusc.2019.01.259

[22] Park, C.H., Jeong, G.H., Theerthagiri, J., Lee, H. and Choi, M.Y. (2023) Moving beyond $Ti_2C_3T_x$ MXene to Pt-Decorated TiO_2@TiC Core-Shell via Pulsed Laser in Reshaping Modification for Accelerating Hydrogen Evolution Kinetics. *ACS Nano*, **17**, 7539-7549. https://doi.org/10.1021/acsnano.2c12638

[23] Novoselov, T., Malinov, S., Sha, W. and Zhechev, A. (2004) High-Temperature Synchrotron X-Ray Diffraction Study of Phases in a Gamma Ti Al Alloy. *Materials Science and Engineering A*, **371**, 103-112. https://doi.org/10.1016/j.msea.2003.12.015

[24] Chen, X., Huang, L., Jiao, Y., Wang, S., An, Q., Bao, Y. and Geng, L. (2021) Mechanisms of Oxidation Anisotropy between α-Ti (0001) and Crystallographic Planes in Titanium Matrix Composites, *Materials Letters*, **286**, Article ID: 129230. https://doi.org/10.1016/j.matlet.2020.129230

[25] Martínez, J., Reyes, D., Vigueras, E., Patiño, C., Reyes, J.A., Castrejón, V.H. and García, I. (2022) Mechanosynthesis of Graphene Nanoribbons from Waste Zinc-Carbon Batteries. *Carbon Letters*, **32**, 475-493. https://doi.org/10.1007/s42823-021-00279-6

[26] Camacho, M., Reyes, D., González, M.A., Camacho, M.A. and Vigueras, E. (2017) Photoluminescent Colloidal Cu@C-NPs Suspensions Synthesized by LASL. *Optics & Laser Technology*, **90**, 102-108. https://doi.org/10.1016/j.optlastec.2016.11.004

[27] Madrigal, M., Vilchis, A.R., Camacho, M. and Camacho, M.A. (2018) Synthesis of MoC@Graphite NPs by Short and Ultra-Short Pulses Laser Ablation in Toluene under N_2 Atmosphere. *Diamond and Related Materials*, **82**, 63-69. https://doi.org/10.1016/j.diamond.2017.12.019

[28] Abdo, N.I. (2021) Comparative Study between Magnetite Nanoparticles and Magnetite/Silver as a Core/Shell Nanostructure. *Advances in Nanoparticles*, **10**, 115-122. https://doi.org/10.4236/anp.2021.104008

[29] Li, Z., Deng, L., Kinloch, I.A. and Young, R.J. (2023) Raman Spectroscopy of Carbon Materials and Their Composites: Graphene, Nanotubes and Fibres. *Progress in Materials Science*, **135**, Article ID: 101089. https://doi.org/10.1016/j.pmatsci.2023.101089

[30] Zhang, X., Lin, Y., Zhang, L., Huang, Z., Yang, L., Li, Z., Yang, Y., Gao, M., Sun, W., Pan, H. and Liu, Y. (2023) Hydrogen-Assisted One-Pot Synthesis of Ultrasmall TiC Nanoparticles Enhancing Hydrogen Cycling of Sodium Alanate. *Chemical Engineering Journal*, **462**, Article ID: 142199. https://doi.org/10.1016/j.cej.2023.142199

[31] Kim, W.J. and Yu, Y.J. (2014) The Effect of the Addition of Multiwalled Carbon Nanotubes on the Uniform Distribution of TiC Nanoparticles in Aluminum Nanocomposites. *Scripta Materialia*, **72**, 25-28. https://doi.org/10.1016/j.scriptamat.2013.10.008

[32] Niwase, K. (2012) Raman Spectroscopy for Quantitative Analysis of Point Defects and Defect Clusters in Irradiated Graphite. *International Journal of Spectroscopy*, **2012**, Article ID: 197609. https://doi.org/10.1155/2012/197609